Title

Amyloid beta-protein: monomer structure and early aggregation states of Abeta42 and its Pro19 alloform.

Journal

Journal of the American Chemical Society, 127(7)

ISSN

0002-7863

Authors

Bernstein, Summer L
Wyttenbach, Thomas
Baumketner, Andrij
et al.

Publication Date

2005-02-01

DOI

10.1021/ja044531p

Peer reviewed

J|A|C|S
ARTICLES
Published on Web 01/29/2005

Amyloid β-Protein: Monomer Structure and Early Aggregation States of Aβ42 and Its Pro[19] Alloform

Summer L. Bernstein,[†] Thomas Wyttenbach,[†] Andrij Baumketner,[†,§] Joan-Emma Shea,[†] Gal Bitan,[‡] David B. Teplow,[‡] and Michael T. Bowers*[,†]

Contribution from the Department of Chemistry and Biochemistry, University of California, Santa Barbara, California 93106-9501, Center for Neurologic Disease, Brigham and Women's Hospital, and Department of Neurology, Harvard Medical School, Boston, Massachusetts 02115, and Department of Neurology, David Geffin School of Medicine, University of California, Los Angeles, California 93005

Received September 9, 2004; E-mail: bowers@chem.ucsb.edu

Abstract: The amyloid β-protein (Aβ) is a seminal neuropathic agent in Alzheimer's disease (AD). Recent evidence points to soluble Aβ oligomers as the probable neurotoxic species. Among the naturally occurring Aβ peptides, the 42-residue form Aβ42 is linked particularly strongly with AD, even though it is produced at approximately 10% of the levels of the more abundant 40-residue form Aβ40. Here, we apply mass spectrometry and ion mobility to the study of Aβ42 and its Pro[19] alloform. The Phe[19] → Pro[19] substitution blocks fibril formation by [Pro[19]]Aβ42. Evidence indicates that solution-like structures of Aβ monomers are electrosprayed and characterized. Unfiltered solutions of Aβ42 produce only monomers and large oligomers, whereas [Pro[19]]Aβ42 solutions produce abundant monomers, dimers, trimers, and tetramers but no large oligomers. When passed through a 10,000 amu filter and immediately sampled, Aβ42 solutions produce monomers, dimers, tetramers, hexamers, and an aggregate of two hexamers that may be the first step in protofibril formation. These results are consistent with recently published photochemical cross-linking data and lend support to recent aggregation mechanisms proposed by Bitan, Teplow, and co-workers [*J. Biol. Chem.* **2003**, *278*, 34882−34889].

Introduction

Substantial experimental evidence supports a seminal role for the amyloid β-protein (Aβ) in Alzheimer's disease (AD).[1] It has been known for over 20 years that plaques composed of these peptides are found in the brain tissue of patients with AD. These observations led researchers to develop what was termed the Amyloid Cascade Hypothesis[2] which held that amyloid plaques were causative agents in the development of AD. Recently, however, increasing numbers of studies have indicated that soluble oligomers of Aβ are neurotoxic even if plaque formation has not occurred,[3−5] leading to a focus on small oligomers and their structure and mechanism of formation.[6] These studies have been greatly assisted by the development of photochemical cross-linking techniques, for example photo-induced cross-linking of unmodified proteins (PICUP),[7,8] allowing the quantitative determination of the Aβ oligomer frequency distribution.[9−11]

Aβ peptides are formed from the amyloid β-protein precursor (AβPP) by endoproteolytic cleavage by a family of secretases. A variety of peptides are formed, the most common of which are 40 and 42 amino acids long, termed Aβ40 and Aβ42, respectively. Although Aβ40 is nearly 10 times as abundant as Aβ42, Aβ42 is generally the predominant species in amyloid plaques. Further, Aβ42 has been shown to have enhanced neurotoxicity relative to that of Aβ40.[12−14] There are a number of naturally occurring alloforms,[15−20] with substitutions usually occurring in or near the central hydrophobic cluster of the

[†] University of California, Santa Barbara.
[‡] Brigham and Women's Hospital, and Harvard Medical School and Department of Neurology; David Geffin School of Medicine, University of California.
[§] Permanent Address: Institute for Condensed Matter Physics, 1 Svientsitsky Str., Lviv 79011, Ukraine.

(1) Selkoe, D. J. *Physiol. Rev.* **2001**, *81*, 741−766.
(2) Hardy, J.; Selkoe, D. J. *Science* **2002**, *297*, 353−356.
(3) Wang, J.; Dickson, D. W.; Trojanowski, J. Q.; Lee, V. M.-Y. *Exp. Neurol.* **1999**, *158*, 328−337.
(4) Klein, W. L.; Krafft, G. A.; Finch C. E. *Trends Neurosci.* **2001**, *24*, 219−224.
(5) Kirkitadze, M. D.; Bitan, G.; Teplow, D. B. *J. Neurosci. Res.* **2002**, *69*, 567−577.
(6) Bitan, G.; Vollers, S. S.; Teplow, D. B. *J. Biol. Chem.* **2003**, *278*, 34882−34889.
(7) Fancy, D. A.; Denison, C.; Kim, K.; Xie, Y. Q.; Holdeman, T.; Amini, F.; Kodadek. T. *Chem. Biol.* **2000**, *7*, 697−708.
(8) Fancy, D. A.; Kodadek, T. *Proc. Natl. Acad. Sci. U.S.A.* **1999**, *96*, 6020−6024.
(9) Bitan, G.; Lomakin, A.; Teplow, D. B. *J. Biol. Chem.* **2001**, *276*, 35176−35184.
(10) Bitan, G.; Kirkitadze, M. D.; Lomakin, A.; Vollers, S. S.; Benedek, G. B.; Teplow, D. B. *Proc. Natl. Acad. Sci. U.S.A.* **2003**, *100*, 330−335.
(11) Bitan, G.; Teplow, D. B. *Acc. Chem. Res.* **2004**, *37*, 357−364.
(12) Younkin, S. G. *Ann. Neurol.* **1995**, *37*, 287−288.
(13) Selkoe, D. J. *Nature* **1999**, *399*, A23-A31.
(14) Dahlgren, K. N.; Manelli, A. M.; Stine, W. B.; Baker, L. K.; Krafft, G. A.; LaDu, M. J. *J. Biol. Chem.* **2002**, *277*, 32046−32053.
(15) Hendriks, L.; van Duijn, C. M.; Cras, P.; Cruts, M.; van Hul, W.; van Harskamp, F.; Warren, A.; McInnis, M. G.; Antonarakis, S. E.; Martin, J. J.; Hofman, A.; van Broeckhoven, C. *Nat. Genet.* **1992**, *1*, 218−221.
(16) Levy, E.; Carman, M. D.; Fernandez-Madrid, I. J.; Power, M. D.; Lieberburg, I.; van Duinen, S. G.; Bots, G. T. A. M.; Luyendijk, W.; Frangione, B. *Science* **1990**, *248*, 1124−1126.
(17) Tagliavini, F.; Rossi, G.; Padovani, A.; Magoni, M.; Andora, G.; Sgarzi, M.; Bizzi, A.; Savioardo, M.; Carrella, F.; Morbin, M.; Giaconne, G.; Bugiani, O. *Alzheimer's Rep.* **1999**, *2* (suppl.), 528.

peptide (residues 17−21). In each instance, disease occurred but with variations in onset, symptoms, and degree of fibrillization. In contrast, the substitution Phe[19] → Pro[19] (F19P) has been shown to prevent fibril formation *in vitro*.[21,22]

Here we present studies of Aβ42 and the associated alloform [Pro[19]]Aβ42 using nanoelectrospray (ESI) mass spectrometry (MS) and ion mobility spectrometry (IMS). Ion mobility[23,24] has become a powerful technique for investigation of conformations of both synthetic[25−27] and biologically interesting polymers,[28−30] and reviews are available.[31,32] Here our goal is to investigate conformational differences in monomers and small oligomers of wild-type and Pro[19]-substituted Aβ42 and to study the energetics and mechanisms of initial oligomerization reactions. PICUP experiments have been done on both peptides,[6] and comparisons are made between results obtained by IMS/MS and PICUP. In addition, comparisons with recent molecular dynamics calculations on Aβ42 are made both to evaluate the calculations and to gain insight into the structure of the Aβ42 monomer.

Materials and Methods

Materials. Wild-type Aβ42 [DAEFRHDSGYEVHHQKLVF[19]FAEDVGSNKGAIIGLMVGGV VIA[42]] and the Pro[19] alloform were synthesized by Fmoc (*N*-(9-fluorenyl)methoxycarbonyl) chemistry, purified by reversed-phase HPLC, and characterized by mass spectrometry and amino acid analysis as previously described.[33] Samples for IMS and MS were prepared by dissolving previously quantified lyophilized peptides in H_2O, sonicating for 1 min, and diluting to a final concentration of 30 μM peptide in 49.5% H_2O, 49.5% acetonitrile, and 1% NH_4OH. (Dissolution at high pH slows down peptide aggregation.[34])

Filtration of Aβ. Certain samples were prepared by filtration through a 10,000 amu gel filtration G-10 Macro Spin column purchased from Nest Group Inc. The filters were hydrated and washed in 10 mM ammonium acetate pH 7.2 according to manufacturer's suggestions. Lyophilized peptide was dissolved at 4 mg/mL in deionized water. To this solution, 0.006 times the volume of 1 N NaOH was added, and then 20 mM ammonium acetate pH 7.2 was added, reducing the peptide concentration to about 2 mg/mL. The solution was sonicated for 1 min because short sonication helps break down preformed aggregates and increase the concentration of the peptide.[35] Then 100 μL was transferred to the filter and spun for 5 min at 2000*g*. The filtrate was collected and used immediately, having a final concentration of 30−50 μM.

Mass Spectrometry. Mass spectra were recorded on a Q-TOF mass spectrometer (Micromass UK Ltd.) equipped with a nanoflow electrospray interface and on a home-built instrument described below.[36] Nano-ESI gold-coated borosilicate capillaries (0.1 mm o.d./0.78 mm i.d.) purchased from Proxeon (Germany) were filled with between 2 and 5 μL of sample solutions for all MS and IMS experiments. All spectra were calibrated using CsI in H_2O at pH 5.0, and mass spectral analysis was performed using MassLynx (Micromass UK Ltd.).

Ion Mobility Experiments. IMS experiments were conducted on a home-built instrument composed of a nano-ESI source, an ion funnel, a temperature-controlled drift cell, and a quadrupole mass filter.[36] Ions are generated continuously from the solution in the nano-ESI source, passed through a capillary, and injected into the ion funnel. The ion funnel is the interface to the vacuum system and can also be used as an ion storage device to convert the continuous ion beam into short ion pulses for cross section measurements. The ion injection energy can be varied from 0 to 150 eV. At low injection voltages, the ions are gently pulsed into the mobility cell and only need a few "cooling" collisions to reach thermal equilibrium with the buffer gas. At high injection voltage, the larger collision energy leads to internal excitation of the ions before cooling and equilibrium occur. This transient internal excitation can lead to annealing, i.e. partial or complete isomerization to the most stable conformers[37] or, if they are present, dissociation of dimers and higher-order oligomers.[37,38]

Once in the cell, the ions are quickly thermalized by collisions with the helium buffer gas present at a pressure (p) of 5 Torr. The ions are drawn through the cell under the influence of a weak electric field. Due to the balance between the force imposed by the electric field (E) and the retarding force of friction, the ions obtain a constant drift velocity (v_D) which is proportional to E with the low field-mobility K being the proportionality constant.[39]

$$v_D = KE \tag{1}$$

The ions exit the drift cell, pass through a quadrupole mass filter, and are detected as a function of time, producing an arrival time distribution. Using kinetic theory,[39] it is possible to relate the ion mobility to the ion collision cross section (σ) and consequently to the arrival time at the detector (t_A).

$$\sigma = 1.3\left(\frac{q^2E^2T}{\mu k_B p^2 N^2 \ell^2}\right)^{1/2}(t_A - t_0) \tag{2}$$

where q is the ion charge, T the temperature, μ the reduced mass of the ion−He collision, N the helium number density at STP, ℓ the cell

(18) Kamino, K.; Orr, H. T.; Payami, H.; Wijsman, E. M.; Alonso, M. E.; Pulst, S. M.; Anderson, L.; O'Dahl, S.; Nemens, E.; White, J. A.; Sadovnick, A. D.; Ball, M. J.; Kaye, J.; Warren, A.; McInnis, M.; Antonarakis, S. E.; Korenberg, J. R.; Sharma, V.; Kukull, W.; Larson, E.; Heston, L. L.; Martin, G. M.; Bird, T. D.; Schellenberg, G. D. *Am. J. Hum. Genet.* **1992**, *51*, 998−1014.
(19) Grabowski, T. J.; Cho, H. S.; Vonsattel, J. P. G.; Rebeck, G. W.; Greenberg, S. M. *Ann. Neurol.* **2001**, *49*, 697−705.
(20) Nilsberth, C.; Westlind-Danielsson, A.; Eckman, C. B.; Condron, M. M.; Axelman, K.; Forsell, C.; Stenh, C.; Luthman, J.; Teplow, D. B.; Younkin, S. G.; Näslund, J.; Lannfelt, L. *Nat. Neurosci.* **2001**, *4*, 887−893.
(21) Wood, S. J.; Wetzel, R.; Martin, J. D.; Hurle, M. R. *Biochemistry* **1995**, *34*, 724−730.
(22) Teplow, D. B.; Lomakin, A.; Benedek, G. B.; Kirschner, D. A.; Walsh, D. M. In *Alzheimer's Disease: Biology, Diagnosis, and Therapeutics*; Iqbal, K., Winblad, B., Nishimura, T., Takeda, M., Wisniewski, H. M., Eds; Wiley: Chichester, UK, 1997; pp 311−319.
(23) (a) von Helden, G.; Hsu, M.-T.; Kemper, P. R.; Bowers, M. T. *J. Chem. Phys.* **1991**, *95*, 3835−3837. (b) von Helden, G.; Hsu, M.-T. Gotts, N.; Bowers, M. T. J. *Phys. Chem.* **1993**, *97*, 8182−8192.
(24) Bowers, M. T.; Kemper, P. R.; von Helden, G.; van Koppen, P. A. M. *Science* **1993**, *260*, 1446−1451.
(25) (a) von Helden, G.; Wyttenbach, T.; Bowers, M. T. *Science* **1995**, *267*, 1483−1485. (b) Gidden, J.; Wyttenbach, T.; Jackson, A. T.; Scrivens, J. H.; Bowers, M. T. *J. Am. Chem. Soc.* **2000**, *122*, 4692−4699.
(26) (a) Gidden, J.; Wyttenbach, T.; Batka, J. J.; Weis, P.; Jackson, A. T.; Scrivens, J. H.; Bowers, M. T.*J. Am. Chem. Soc.* **1999**, *121*, 1421−1422. (b) Gidden, J.; Wyttenbach, T.; Jackson, A. T.; Scrivens, J. H.; Bowers, M. T. *J. Am. Soc. Mass Spectrom.* **1999**, 10, 883−895.
(27) Gidden, J.; Kemper, P. R.; Shammel, E.; Fee, D. P.; Anderson, S.; Bowers, M. T. *Int. J. Mass Spectrom.* **2003**, *222*, 63−73.
(28) (a) Wyttenbach, T.; von Helden, G.; Bowers, M. T. *J. Am. Chem. Soc.* **1996**, *118*, 8355−8364. (b) Wyttenbach T.; Bushnell J. E.; Bowers, M. T. *J. Am. Chem. Soc.* **1998**, *120*, 5098−5103. (c) Gidden, J.; Bushnell, J. E.; Bowers, M. T. *J. Am. Chem. Soc.* **2001**, *123*, 5610−5611.
(29) (a) Shelimov, K. B.; Jarrold, M. F. *J. Am. Chem. Soc.* **1997**, *119*, 2987−2994. (b) Hudgins, R. R.; Woenckhaus, J.; Jarrold, M. F. *Int. J. Mass Spectrom. Ion Proc.* **1997**, *165/166*, 497−507. (c) Jarrold, M. F. *Acc. Chem. Res.* **1999**, *32*, 360−367. (d) Mao, Y.; Woenckhaus, J.; Kolafa, J.; Ratner, M. A.; Jarrold, M. F. *J. Am. Chem. Soc.* **1999**, *121*, 2712−2721.
(30) (a) Badman, E. R.; Hoaglund-Hyzer, C. S.; Clemmer, D. E. *Anal. Chem.* **2001**, *73*, 6000−6007. (b) Myung, S.; Badman, E. R.; Lee, Y. J.; Clemmer, D. E. *J. Phys. Chem. A.* **2002**, *106*, 9976−9982.
(31) Clemmer, D. E.; Jarrold, M. F. *J. Mass Spectrom.* **1997**, *32*, 577−592.
(32) Wyttenbach, T.; Bowers, M. T. *Top. Curr. Chem.* **2003**, *225*, 207−232.
(33) Lomakin, A.; Chung, D. S.; Benedek, G. B.; Kirschner, D. A.; Teplow, D. B. *Proc. Natl. Acad. Sci. U.S.A.* **1996**, *93*, 1125−1129.
(34) Fezoui, Y.; Hartley, D. M.; Harper, J. D.; Khurana, R.; Walsh, D. M.; Condron, M. M.; Selkoe, D. J.; Lansbury, P. T.; Fink, A. L.; Teplow, D. B. *Amyloid* **2000,** *7*, 166−178.
(35) Stathopulos, P. B.; Scholz, G. A.; Hwang, Y.-M.; Rumfeldt, J. A. O.; Lepock, J. R.; Meiering, E. M. *Protein Sci.* **2004**, *13*, 3017−3027.
(36) Wyttenbach, T.; Kemper, P. R.; Bowers, M. T. *Int. J. Mass Spectrom.* **2001**, *212*, 13−23.
(37) (a) von Helden, G.; Gotts, N. G.; Bowers, M. T. *Nature* **1993**, *363*, 60−63. (b) von Helden, G.; Gotts, N. G.; Bowers, M. T. *J. Am. Chem. Soc.* **1993**, *115*, 4363−4364.
(38) Liu, D.; Wyttenbach, T.; Carpenter, C. J.; Bowers, M. T. *J. Am. Chem. Soc.* **2004**, *126*, 3261−3270.
(39) Mason, E. A.; McDaniel, E. W. *Transport Properties of Ions in Gases*; Wiley: New York, 1988.

length, k_B the Boltzmann constant, and t_0 the time the ion spends after exiting the cell before hitting the detector. Since all of the constants in eq 2 are known for a given experiment and t_A and t_0 can be very accurately measured, a precise value of σ is obtained.

Molecular Dynamics. Extensive molecular dynamics on Aβ42 monomer were performed using the "replica exchange"(REX) protocol[40] within the CHARMM set of programs[41] to obtain a thermal distribution of Aβ42 structures. Initially REX calculations were performed on Aβ42 in implicit water solvent (GB/SA),[42] yielding a distribution of hydrated structures. A second set of structures was obtained by reoptimizing the structures of the first set in a solvent-free environment to mimic the rapid dehydration that occurs in the ESI experiment. Finally, a third distribution of structures was generated using the REX protocol on Aβ42 initiated in a completely solvent-free environment to obtain equilibrated gas-phase structures. Cross sections of the model structures can be calculated either by using a modified projection method[43] or by using a more sophisticated scattering method.[44] Details of these calculations are given elsewhere.[45]

Results

Mass Spectra. Typical nano-ESI spectra for Aβ42 and [Pro^{19}]Aβ42 taken on the Q-TOF mass spectrometer are given in panels a and b of Figure 1, respectively. The dominant peak in each spectrum corresponds to an *m*/*z* appropriate for the −3 charge state of the monomer. The result is consistent with primary structures of these peptides which have three basic sites and six acidic sites at neutral pH. The peaks at *m*/*z* values appropriate for the −4 and −5 monomer charge states could be due to excess charging occurring in the electrospray process although some or all of the −4 charge state could have originated from solution.

In the Aβ42 spectrum (Figure 1a), there are very small peaks that correspond to monomer charge states of −5/2 and −2. Clearly the −5/2 charge-state peak must come from a dimer (or higher-order oligomer). These two charge states are strongly enhanced in the spectrum of [Pro^{19}]Aβ42. In addition, a weak peak at monomer charge state −7/3 is also observed, indicating the presence of trimer in the [Pro^{19}]Aβ42 spectrum. The fact that a peak is not present at a monomer charge state of −7/2 indicates dimer ions preferentially carry either the same or less proportional charge than monomer ions, a fact consistent with literature observations in other systems.[46] It also suggests that the −4 monomer is probably a minor species in solution for [Pro^{19}]Aβ42.

To obtain further information on the nature of the observed mass spectral peaks, ^{13}C isotope distributions were measured. These are shown for the −3 and −2 monomer charge states[47] of [Pro^{19}]Aβ42 in Figure 1b. The isotope peak separation for the −3 charge state is precisely 0.33 amu—as expected for a monomer. Since we could not baseline resolve the isotope

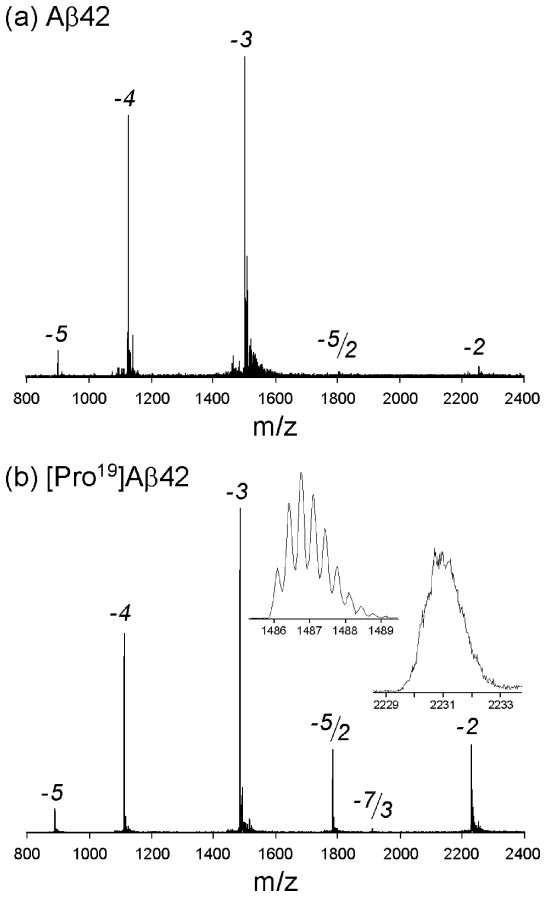

Figure 1. Mass spectra of Aβ-peptides. (a) Wild-type Aβ42 taken from an unfiltered solution at 30 μM concentration near pH 8. The putative monomer charge states of −2, −3, −4, and −5 are indicated along with a −5/2 peak. (b) The Pro^{19} alloform of Aβ42. The two insets are high-resolution spectra of the −3 and −2 charge states. The −5/2 peak would correspond to a putative −5 dimer and the small −7/3 peak to a −7 trimer.

multiplet, some fraction of −6 dimer (and/or higher-order oligomers) cannot be ruled out. The isotope distribution for the −3 charge state in Figure 1b is in quantitative agreement with the predicted ^{13}C,^{15}N distribution for Aβ42, confirming this charge state is primarily monomer.

A similar high-resolution spectrum for the −2 charge-state peak is also given in Figure 1b. In this case, no discernible structure is observed. If this peak were dominantly monomer, a ^{13}C isotope separation of 0.5 amu should have been observed. Hence, higher-order oligomers likely are present in this peak. To investigate this possibility, a collision-induced dissociation (CID) experiment was run using the Q-TOF mass spectrometer. The −2 charge state peak was selected by the quadrupole and subjected to low-energy CID by adding Ar gas to the collision cell located between the selection quadrupole and the TOF analyzer. If trimer and dimer comprise part of this feature, as suggested by the data in Figure 2a, then the following CID processes could occur.

$$([\text{Pro}^{19}]\text{A}\beta42)_3^{6-} \rightarrow ([\text{Pro}^{19}]\text{A}\beta42)_2^{4-} + ([\text{Pro}^{19}]\text{A}\beta42)^{2-}$$

$$([\text{Pro}^{19}]\text{A}\beta42)_2^{4-} \rightarrow 2([\text{Pro}^{19}]\text{A}\beta42)^{2-}$$

The high-resolution spectrum of the −2 charge state following CID is given in Figure 2b. Clearly, a well-resolved series of peaks separated by 0.5 amu is observed, indicating the −2

(40) Sugita, Y.; Okamoto, Y. *Chem. Phys. Lett.* **1999**, *314*, 141−151.
(41) MacKerell, A. D., Jr.; Bashford, D.; Bellott, R. L.; Dunbrack, R. L., Jr.; Evanseck, J. D.; Field, M. J.; Fischer, S.; Gao, J.; Guo, H.; Ha, S.; Joseph-McCarthy, D.; Kuchnir, L.; Kuczera, K.; Lau, F. T. K.; Mattos, C.; Michnick, S.; Ngo, T.; Nguyen, D. T.; Prodhom, B.; Reiher, W. E., III; Roux, B.; Schlenkrich, M.; Smith, J. C.; Stote, R.; Straub, J.; Watanabe, M.; Wiorkiewicz-Kuczera, J.; Yin, D.; Karplus, M. *J. Phys. Chem. B* **1998**, *102*, 3586−3616.
(42) Lee, M. S.; Salsbury, F. R., Jr.; Brooks, C. L., III. *J. Chem. Phys.* **2002**, *116*, 10606−10614.
(43) Wyttenbach, T.; von Helden, G.; Batka, J. J., Jr.; Carlat, D.; Bowers, M. T. *J. Am. Soc. Mass Spectrom.* **1997**, *8*, 275−282.
(44) (a) Mesleh, M. F.; Hunter, J. M.; Shvartsburg, A. A.; Schatz, G. C.; Jarrold, M. F.; *J. Phys. Chem.* **1996**, *100*, 16082−16086. (b) Shvartsburg, A. A.; Jarrold, M. F. *Chem. Phys. Lett.* **1996**, *261*, 86−91.
(45) Baumketner, A.; Shea, J.-E.; Wyttenbach, T.; Bernstein, S.; Bitan, G.; Teplow, D. B.; Bowers, M. T. Manuscript in preparation.
(46) See, for example: Nettleton, E. J.; Tito, P.; Sunde, M.; Bouchard, M.; Dobson, C. M.; Robinson, C. V. *Biophys. J.* **2000**, *79*, 1053−1065.

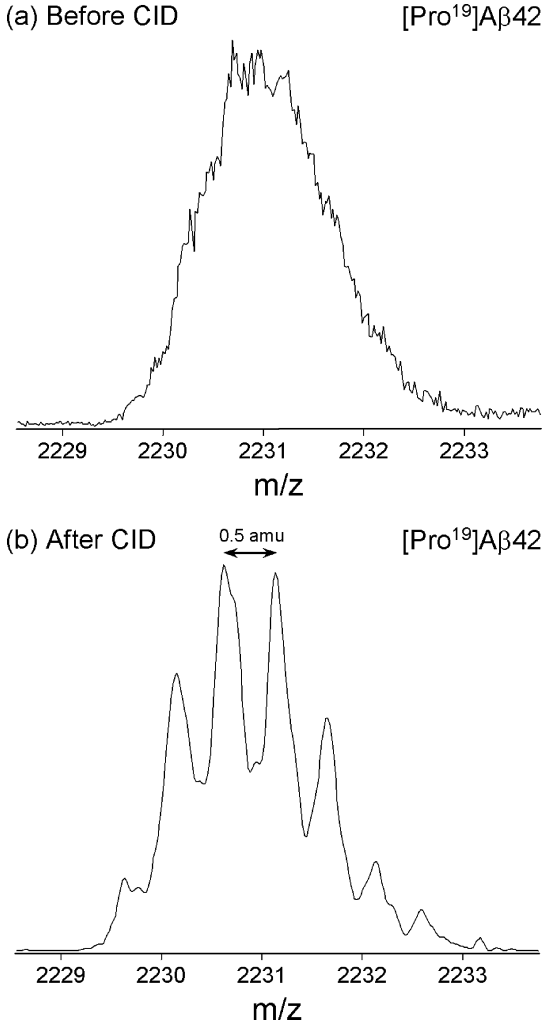

Figure 2. High-resolution mass spectra of the −2 charge state of the [Pro[19]]Aβ42 peptide (a) without Ar collision gas in the collision cell between the quadrupole and TOF analyzer and (b) with Ar in the collision cell.

monomer is now the dominant species present. Small peaks are observed at 0.25 amu separation, indicating that some undissociated dimer remains. The fact that a series of peaks separated by 0.25 amu was not originally observed indicates that the −2 charge state contains components larger than the dimer, such as the −6 trimer, as suggested above.

The Aβ42 peptide clogged the nano-ESI spray tip much more rapidly than the Pro[19] alloform. This result suggests that formation of large aggregates occurs faster for the wild-type peptide. Since a significant amount of dimer is not observed under normal conditions for the wild-type peptide (Figure 1a), the implication is that dimer self-associates rapidly to form higher-order oligomers not observable in our experiment. This qualitative observation is consistent with PICUP results that indicate wild-type peptide forms abundant higher-order oligomers, while the Pro[19] alloform does so to a much lesser extent.[6] When the Aβ42 mass spectrum was obtained immediately following filtration to eliminate species above mass 10,000, a

(47) Throughout this paper, the various features will be referred to by their nominal monomer charge states. It is not intended to imply that these species are pure monomers or even contain the monomer, which is clearly impossible for the −5/2 charge state. However, it does avoid both awkward language and ambiguity in identifying the mass spectral features we are discussing.

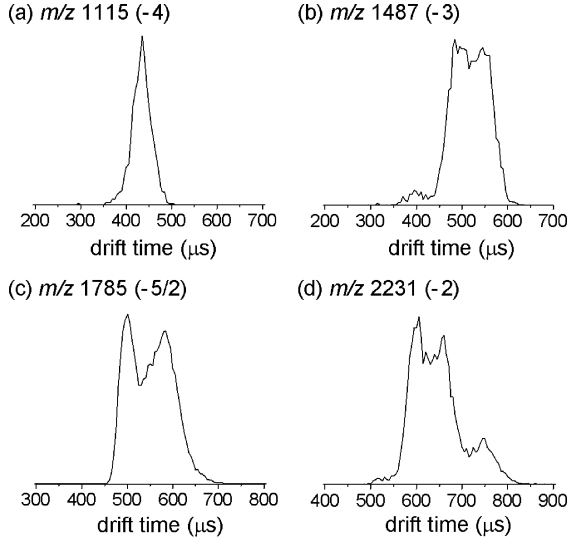

Figure 3. Arrival time distributions for the major features in the mass spectrum of the [Pro[19]]Aβ42 peptide given in Figure 1b. The *m*/*z* values and putative monomer charge states (in brackets) are given. The injection energy was 40 eV in all cases.

significant peak at charge state −5/2 was observed (see Supporting Information).

Arrival Time Distributions. The ability to measure ATDs provides a powerful complementary tool to a mass spectrum. Complex structure (two or more peaks) in an ATD indicates that either a single species is present with at least two noninterconverting conformations or multiple species are present (monomer, dimer, etc.) or both possibilities occur. It is useful to consider a general case before interpreting the experimental ATDs presented in Figures 3−5. For any given integer charge state, $-q$, observed in a mass spectrum, the following species could be present: M^{q-}, D^{2q-}, Tr^{3q-}, ..., where M is the monomer, D is the dimer, Tr the trimer, etc. Each of these species has the same m/q value, and hence, they are indistinguishable in the mass spectrum. They can be distinguished in an ATD, however, since their charge-normalized cross sections will differ. It will almost always be the case that the cross section for the dimer will be less than twice the cross section for the monomer. This fact is apparent if you consider the sum of the cross sections of two isolated monomers versus the cross section of the two monomers stuck together as a dimer. Said another way, $\sigma_D/2q < \sigma_M/q$. The only time this would not be true is if one or both of the monomers unraveled upon forming the dimer, thus resulting in an extended structure; however, this is a physically unreasonable process and has not been observed experimentally.[32,36] It is much more likely that the two species will retain a structure similar to their monomeric structures upon dimerization. In addition, they could partially intertwine. Either of these possibilities yields a smaller charge-normalized cross section than the monomer. This argument continues for larger oligomers yielding $\sigma_{n+1}/(n+1)q < \sigma_n/nq$ where $n = 1$ is the monomer, $n = 2$ is the dimer, etc. This point will be important in interpreting the ATDs of various charge states.

The ATDs for the main peaks of the [Pro[19]]Aβ42 mass spectrum in Figure 1b are shown in Figure 3. The simplest ATD is that for *m*/*z* 1115 (−4 monomer charge state) which is composed of a single peak. The isotope splitting in the mass spectrum (data not shown) is consistent with an assignment of the species as a monomer. The interpretation of the ATD is

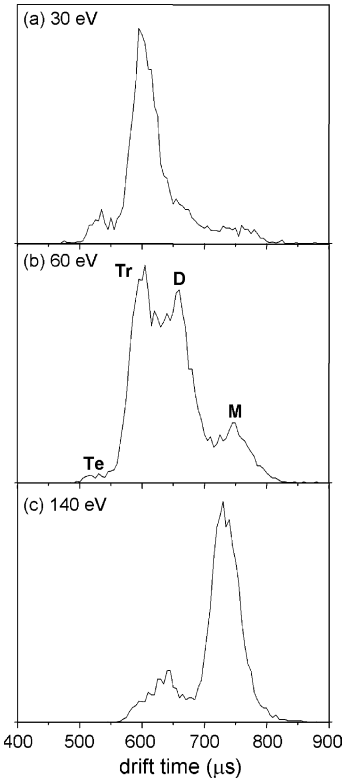

Figure 4. Arrival time distributions for the putative −2 monomer charge state of the [Pro[19]]Aβ42 peptide at the injection energies noted. The peak designations in (b) are M = monomer, D = dimer, Tr = trimer, and Te = tetramer.

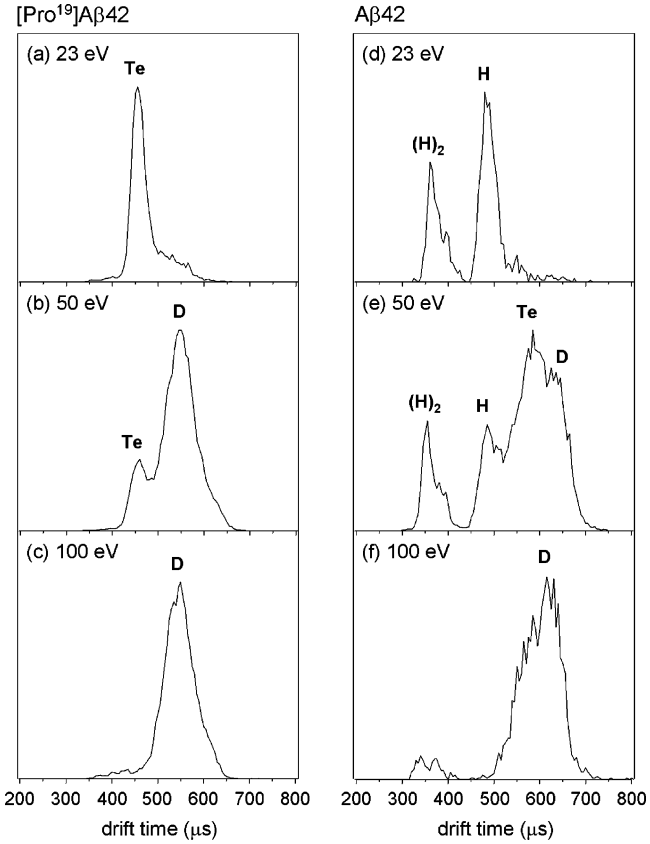

Figure 5. Arrival time distributions for the peptides [Pro[19]]Aβ42 (a−c) and Aβ42 (d−e) for the −5/2 charge states at the injection energies indicated. The letter designations given for the features are D = dimer, Te = tetramer, and H = hexamer.

that there is a single family of similar structures that rapidly interconvert on the experimental time scale (∼1 ms).

The ATD for the *m*/*z* 1487 peak (−3 monomer charge state) is more complex. It is characterized by two large peaks at 490 and 540 μs (each somewhat broader than expected for a single species) and a small peak at 400 μs. The isotope pattern in the mass spectrum (Figure 1b) indicates this ATD is due primarily to monomer. Consequently the two largest peaks must be predominantly monomer. Since these features are resolved, they must represent structures that are sufficiently different in character that they do not interconvert on the millisecond time scale. One possibility is that the 540 μs peak is due to a solution-like structure, and the 490 μs peak, a solvent-free structure. The small peak at 400 μs is assigned to an oligomer.

The ATD for *m*/*z* 1785 (−5/2 charge state) is clearly bimodal. Since we know this peak cannot be monomer, the two simplest interpretations are the following: (1) there are two stable, noninterconverting −5 dimer structures, or (2) the 580 μs peak is a −5 dimer and the 500 μs peak is a −10 tetramer. The latter interpretation is favored for reasons to be discussed later.

Finally, the ATD for the peak at *m*/*z* 2231 (−2 charge state) is the most complex of the lot. We know this peak is predominantly oligomer from the isotope-splitting measurements (Figure 2) discussed previously. Hence, the two large central peaks at 600 and 650 μs are most likely oligomers (dimers and trimers). The small peak at 740 μs could be the −2 monomer, and the smallest peak at 525 μs would be a higher-order oligomer.

ATDs for the −4 and −3 charge states of the Aβ42 species are very similar to each other and to the −3 charge state of [Pro[19]]Aβ42 (data not shown for the −4 charge state; see Supporting Information for the −3 charge state ATD). There are two peaks of similar intensity in the ATD of the −4 charge state of Aβ42 but no smaller peak at shorter times. This result contrasts with the ATD of the −4 charge state of the Pro[19] alloform (Figure 3) where only one peak was observed. We have not yet been able to create experimental conditions where sufficient −2 charge state of Aβ42 is generated to get reliable ATDs. The −5/2 charge state ATD of Aβ42 will be discussed shortly.

ATD Dependence on Injection Energy. Ions stored in the ion funnel can be pulsed into the mobility cell with voltage *V* and resultant translational energy *qV*. This translational energy is rapidly dissipated by collision with the bath gas, and a significant fraction of it is turned into internal energy of the injected ion. This internal energy is then (more slowly) removed by further collisions. This whole process occurs in the first millimeter of the cell, and hence the measured ATDs reflect the nature of the species following the collisional heating/cooling process. Two processes can occur during this transient heating cycle: the ion can anneal to a more stable structure or, if it is an oligomer, can dissociate with both mass and charge evenly divided in the products. (Asymmetric dissociation in either mass or charge would remove the signal due to the fixed *m*/*z* of the quadrupole.)

The injection energy dependence of the −2 charge state of [Pro[19]]Aβ42 is given in Figure 4. There are multiple peaks in the ATDs that change systematically with injection energy. The peak at 740 μs totally dominates the ATD at the highest injection energy (140 eV) but is a minor feature at lower injection

energies. We know from the isotope data in Figure 2 that collisional activation results in oligomer dissociating to monomer for this charge state. Hence, it is reasonable to assign the 740 μs peak to the monomer.

At intermediate injection energies (60 eV), there are three peaks located at shorter times than the monomer. The lack of resolution of the isotope pattern (Figure 2) is strong evidence that species larger than dimer are present in this peak. Hence, it is reasonable to assign the 650 μs peak to the -4 dimer and the 590 μs peak to the -6 trimer. A small amount of a higher-order oligomer (probably tetramer) is present at shortest times. This trend continues for the lowest injection energy (30 eV) where the trimer becomes the dominant feature.[48]

A similar scenario occurs for the $-5/2$ charge state. The data for both the Aβ42 and [Pro^{19}]Aβ42 peptides are shown in Figure 5. First consider the highest injection energy panels (100 eV). For [Pro^{19}]Aβ42 there is a dominant peak at 550 μs and a weak feature near 450 μs. However, for Aβ42 there is a broad feature at long times composed of at least two peaks, one near 620 μs and a shoulder at 580 μs. There is also a weak feature near 350 μs. Since monomers cannot be involved, it is reasonable to assign the 550 μs species in [Pro^{19}]Aβ42 as a dimer with a similar assignment for the 620 μs peak in Aβ42. At 50 eV injection energy there are still two peaks for [Pro^{19}]Aβ42, with the shorter-time peak at 450 μs now substantially larger. It is reasonable to assign the 450 μs peak to the -10 tetramer. A similar assignment can be made for the 580 μs peak in Aβ42, which is now clearly resolved. In addition, a peak at 500 μs is clearly apparent for Aβ42, and the feature at 350 μs is much stronger. This new peak at 500 μs is assigned as the -15 hexamer. At 23 eV injection energy, the Aβ42 ATD is dominated by the hexamer at 500 μs with clear evidence of higher-order oligomers present near 350 μs. In contrast, the [Pro^{19}]Aβ42 ATD shows essentially no signs of oligomerization above the tetramer even at 23 eV injection energy, although a tiny amount of hexamer may be present near 400 μs.

ATD Dependence on Temperature. Obtaining the temperature dependence of ATDs is much more difficult to execute than injection energy studies due to the long time it takes to have the system equilibrate once the temperature is changed. This has made study of the temperature dependence of the ATDs of Aβ42 difficult. Nevertheless, data were obtained for the [Pro^{19}]Aβ42 $-5/2$ charge state system over a significant temperature range. Examples are shown in Figure 6. The absolute values of the $-5/2$ peak in the mass spectra at the various temperatures were used to normalize the ATD data. Relative abundances were obtained by integrating the areas under the curves for the two peaks in the ATD at each temperature.

The tetramer peak decreases most rapidly with increasing temperature and is no longer observed at 452 K. The dimer initially decays slowly (possibly due to partial "restocking" from the dissociating tetramer), then begins a steep descent near 440 K, and disappears at 510 K. Arrhenius analysis yields activation energies for dissociation of 18.3 (tetramer) and 20.4 kcal/mol (dimer) and preexponential A factors of 4.4 and 4.2 s^{-1}, respectively.

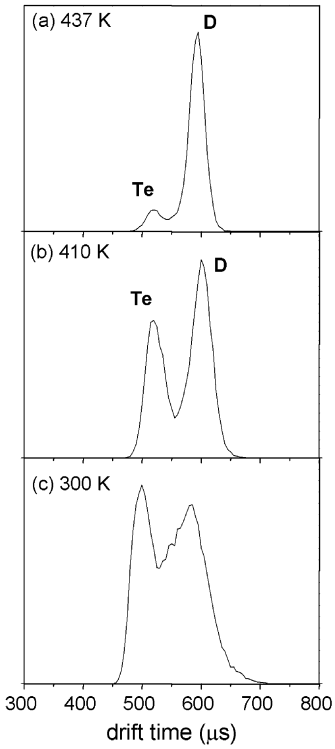

Figure 6. Arrival time distribution of the $-5/2$ charge state of the [Pro^{19}]Aβ42 peptide at the temperatures indicated. The injection energy was 40 eV. The letters above the peaks stand for D = dimer and Te = tetramer.

Modeling. Only the monomer of the Aβ42 peptide in the -3 charge state has been modeled to date. The details of the calculation and an in-depth analysis of the structural implications are being reported elsewhere.[45] Here we will only comment on the overall cross sections and the implication these have for assigning experimental peaks in the -3 charge state ATD.

Three calculations were done. The first was done in an implicit water solvent environment and yielded an average cross section of 840 Å^2. When the structures were dehydrated and reminimized, the average cross section was reduced to 760 Å^2. Finally, a calculation was done assuming a solvent-free environment. Under these conditions, more compact structures were obtained with an average cross section of 680 Å^2.

Typical structures from the three different calculations are shown in Figure 7. Some important structural aspects are demonstrated. First, the hydrated (panel a) and dehydrated (panel b) structures are highly similar. The latter is somewhat more compact since the polar groups utilize intramolecular interactions to replace the stabilizing effects of the water. In these two structures, the hydrophobic tail and hydrophobic core strongly interact and are located predominantly in the peptide interior. Although these hydrophobic segments are predominantly on the peptide interior, Aβ42 is not large enough to completely bury them; as a result a hydrophobic component remains exposed. This could be an important driving force in aggregation of Aβ42.[6,49,50]

(48) A word of caution must be given, however, for data at these lowest injection energies. Below 30 or 40 eV injection energy, discrimination against larger species can occur. This happens due to collisional scattering of the species trying to enter the cell from the ion funnel; the larger the cross section of the species, the more the scatter and the lower the transmission. Hence, while the trend toward higher-order oligomers most probably continues below 60 eV, the quantitative distribution of components in the peaks becomes less certain. This is unfortunate because, as the injection energy is lowered, less collisional dissociation or conformational annealing occurs, and hence, a more accurate picture emerges of the oligomer distribution in solution. On balance, considering all of the evidence, the nominal -2 monomer peak being sprayed from solution is dominated by dimer and trimer.

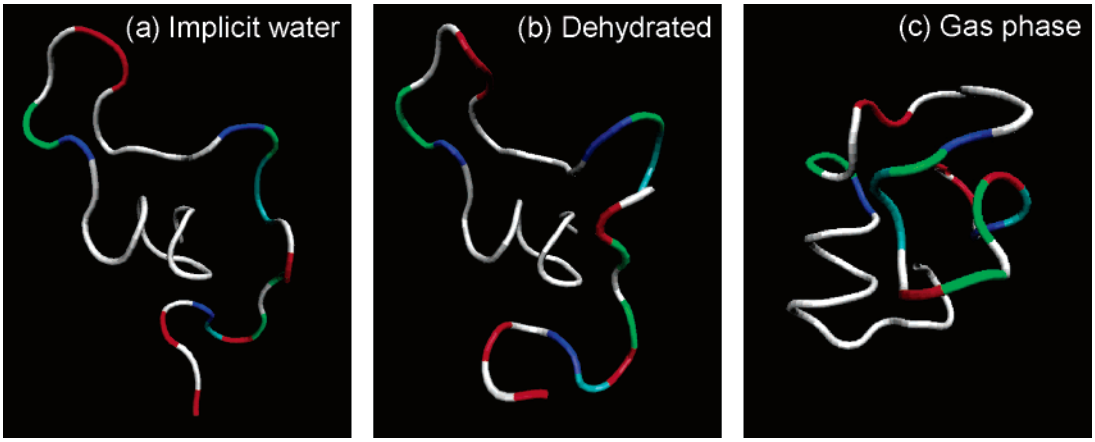

Figure 7. Typical model structures for the hydrated, dehydrated, and solvent-free families of structures of Aβ42. The hydrophobic residues are shown in gray and the hydrophilic residues in red and blue. Note the similarities between the hydrated and dehydrated structures and the interaction of the hydrophobic core and hydrophobic tail.

The solvent-free conformation is much more compact than the hydrated conformation and has essentially turned Aβ42 inside out. The hydrophobic parts are now on the exterior of the peptide and no longer interact with each other. The charges and polar side chains are buried in the peptide interior, providing good self-solvation.

The ATD for the −3 charge state of Aβ42 (Supporting Information) is essentially identical to that of [Pro[19]]Aβ42 (Figure 3b). The two main peaks have cross sections of 700 and 640 Å^2. Since these both must be predominantly monomer, as indicated by isotope distribution studies (data not shown), and since they do not interconvert on the millisecond time scale, two very different monomer structures are being detected. These data are consistent with the larger cross section component corresponding to a dehydrated solution structure and the smaller cross section component being due to a solvent-free gas-phase structure. The predicted cross sections from the calculations are about 8% larger than experimental cross sections. This is a somewhat larger discrepancy than typically found for smaller systems,[25−28] but considering the size and complexity of Aβ42 it is satisfactory.[51] The relative difference in cross sections are considerably better, with theory predicting the solution-type dehydrated structures to be 11% larger than the gas phase and experiment indicating a difference of 9%.

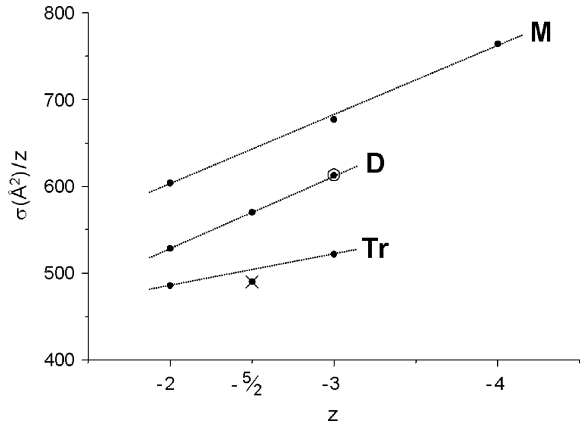

Figure 8. Plot of a charge-normalized cross section versus charge state for the [Pro[19]]Aβ42 peptide. The lines are drawn through the points to guide the eye. The circle drawn around the middle point of the −3 charge state indicates both a monomer and dimer contribute. The point with an × across it for the −5/2 charge state is a tetramer (see text). M = monomer, D = dimer, and Tr = trimer.

Cross Section Measurements. Another aid in assigning peaks in ATDs is to compare the cross sections measured for various peaks in the ATDs of different charge states. This is done in Figure 8 for the [Pro[19]]Aβ42 system (where the broadest set of charge states is observed). There is a linear correlation between the peaks at largest cross sections for the −2, −3, and −4 charge states. Since we have argued a dehydrated solution monomer structure corresponds to this peak for the −3 charge state in Aβ42 and since the ATDs for Aβ42 and [Pro[19]]Aβ42 are essentially identical for the −3 charge state, then it is reasonable to assign the largest cross section for [Pro[19]]Aβ42 to a monomer with solution-like structure. The correlation would then imply solution-like structures for the −2 and −4 monomers as well. The increase in experimental cross section with charge state is a commonly observed feature and is almost certainly due to Coulombic repulsion. The fact that the −4 charge state has a solution-like structure indicates either that it is sprayed directly from solution or that additional charging of the −3 charge state during the spray process retains the solution structure.

There is also a near linear correlation in the next-highest cross section set of structures, for the −2, −5/2, and −3 charge states. For the −5/2 charge state this peak was assigned as dimer. On

(49) Zhang, S.; Iwata, K.; Lachenmann, M. J.; Peng, J. W.; Li, S.; Stimson, E. R.; Lu, Y.; Felix, A. M.; Maggio, J. E.; Lee, J. P. *J. Struct. Biol.* **2000**, *130*, 130−141.
(50) Dobson, C. M. *Nature* **2003**, *426*, 884−890.
(51) There are two factors not taken into account that could lower the theoretical cross sections and improve agreement. The first of these involves doing short dynamics runs on the 355 minimized structures that would not globally rearrange the peptide but would sample nearby configuration space. There is no reason to believe that simply removing the water and minimizing actually locates the favored structures for the dehydrated peptide. These calculations would most probably produce a more compact cohort of structures as potentially more favorable intramolecular stabilization of the charge centers occurs. The second reason is technical. There are several methods available for calculating cross sections for peptides. For smallish systems (20 or fewer amino acids), the projection protocol sigma[43] has been shown to give very accurate results.[26−28] For large systems, or systems with complex (nonspherical) structures, a more sophisticated scattering calculation must be done. There are two flavors for these calculation. For quite large peptides/proteins, a hard sphere ion−helium potential is adequate,[44b] but for intermediate sizes an interaction potential must be included.[44a] Aβ42 is in the awkward size range where one is not certain which method is best. The full scattering method with interaction potential[44a] was used to generate the cross sections reported here. The projection method gives values about 10% smaller. The experimental data fall between the determinations of the two methods, but both give relative cross sections in excellent agreement with experiment.

the basis of injection energy studies, the corresponding peak in the −2 charge state also was assigned as a dimer. Assignment of the peak in the −3 charge state is more complex. Isotopic measurements indicate the −3 charge state is predominantly monomer (Figure 1). However, injection energy studies indicate that the feature at this cross section decreases as injection energy increases relative to the pure monomer feature at highest cross section (data not shown). Theory suggests that, for Aβ42, this peak has a cross section appropriate for a solvent-free monomer. It is reasonable to assume that the [Pro^{19}]Aβ42 alloform has a similar compact solvent-free structure. Hence, the ATD at this cross section likely is a composite of a −6 dimer and a −3 monomer with a compact solvent-free structure. Consequently, we have placed a circle around this data point to indicate it comprises two different species.

The correlation for the smallest cross section points in Figure 8 is not as good as for the monomer and dimer. We have assigned the cross section for the −5/2 charge state to the −10 tetramer. From the spacings in the ATDs of the −2 and −3 charge states, the lowest cross section points are assigned as trimers. Hence, the line is drawn through these two points only. The cross section for the −5/2 charge state falls significantly below this line, supporting its assignment as a tetramer rather than as a trimer.

A similar analysis for the Aβ42 system would be useful. However, we have not yet been able to obtain sufficient intensity for the −2 charge state to acquire reliable ATDs and cross section data. Without these data points, correlations cannot be made reliably.

Discussion

Aβ assembly is a seminal feature of Alzheimer's disease.[1] An increasing body of evidence supports the hypothesis that oligomeric assemblies of Aβ are key pathogenic effectors of the disease.[3−5,52] Recent studies have shown a strong correlation between brain levels of Aβ42 oligomers and AD.[53] Aβ42 also has been shown to be particularly neurotoxic relative to Aβ40, its more abundant alloform.[14] Understanding Aβ42 oligomerization thus has special relevance to efforts to identify therapeutic targets for AD. Unfortunately the dynamic noncovalent, homotypic self-association of Aβ42 presents problems for biochemical and functional analyses. Aβ42 monomer exists in steady state with higher-order assemblies.[9] This situation complicates quantitative determination of the oligomer size distribution and determination of structure−activity relationships (viz., neurotoxicity). The propensity of Aβ to form fibrils also precludes application of classical structure-determination methods, including solution-phase NMR and X-ray crystallography, to the problem of the structural biology of Aβ monomer and oligomers. Here we demonstrate that IMS/MS can provide unique insights into the oligomerization behavior of Aβ42 through its ability to resolve systems of identical *m*/*z* into unique structural elements. These results not only provide insight into the oligomerization mechanism but also generate structural constraints for *in silico* modeling of Aβ assembly.

An important issue is the correlation between what is observed in the IMS/MS experiments and what exists in solution. The mass spectra in Figure 1 for both Aβ42 and [Pro^{19}]Aβ42 have −4 and −3 charge states present but the [Pro^{19}]Aβ42 spectrum has additional peaks at −5/2 and −2 charge states. Isotopic distributions indicate that the −4 and −3 charge states involve primarily monomer, but the −5/2 and −2 charge states are composed of primarily dimers, trimers, and tetramers. If the −5/2 and −2 charge states of [Pro^{19}]Aβ42 had formed during the spray process, they would have been apparent in both mass spectra. Hence, the oligomers observed reflect genuine solution-phase assemblies.

At physiological pH, Aβ42 monomer is expected to be primarily in the −3 charge state due to its amino acid composition. The presence of a significant −4 peak (and at times also a small −5 peak) suggests that a fraction of the monomer observed in the mass spectra may form during the spray process. Hence, there could be a mixture of structures present in the monomer portion of the sprayed peptide. Comparison of the cross section data for the −3 charge state with the modeling results is consistent with this view. Two noninterconverting families of structures are present in the ATD of the −3 charge state: a solution-type structure and a gas-phase structure. However, dimer also contributes to the −3 charge state ATD. This interpretation is consistent with the fact that at highest injection energies, the shorter-time component decreases in intensity relative to the longer-time component (Supporting Information). The spacing between the two peaks in the ATD is consistent either with two monomer conformations (according to theory) or with monomer and dimer (see the data for the −2 charge state in Figure 4).

The injection energy data in Figure 4 for the nominal −2 monomer peak of [Pro^{19}]Aβ42 demonstrate that at highest injection energies, a dominant peak emerges at longest times. This peak must be the −2 monomer. The isotope patterns observed before and after CID (Figure 2) support this assignment. As the injection energy is lowered, prominent new peaks appear at shorter times indicating the presence of other species. These cannot be monomers both because the isotope data in Figure 2 preclude it and because increasing injection energy results in the largest cross section species dominating. Hence, the only possibility is that these peaks correspond to oligomers. The four components in the −2 charge state ATD are then assigned as −2 monomer (minor), −4 dimer (major), −6 trimer (major), and −8 tetramer (minor). These designations are shown on the 60 eV injection ATD (Figure 4).

The ATDs of the −5/2 charge state are distinct from those for the −5/2 charge state of [Pro^{19}]Aβ42 (Figure 5). For [Pro^{19}]Aβ42, there are only two peaks at all injection energies assigned as dimer and tetramer. In contrast, for Aβ42 there are 5 or 6 peaks. The three-peak cluster at long times has been assigned to dimer, tetramer, and hexamer. The peak at shortest times must be a higher-order oligomer. This assignment is supported by the fact that these higher-order oligomers do not fully dissociate even at highest injection energies where the hexamer is completely gone and much of the tetramer has become dimer. Since there are no features between the peak assigned as $(H)_2$ and the broadened peak at longest times in the 100 eV ATD, the putative $(H)_2$ peak does not lose dimer pieces when it gets energized by collision. This fact supports a structure composed of two hexamer units where an entire H unit must

(52) Klein, W. L.; Stine, Jr., W. B.; Teplow, D. B. *Neurobiol. Aging* **2004**, *25*, 569−580.
(53) Gong, Y.; Chang, L.; Viola, K. L.; Lacor, P. N.; Lambert, M. P.; Finch, C. E.; Krafft, G. A.; Klein, W. L. *Proc. Natl. Acad. Sci. U.S.A.* **2003**, *100*, 10417−10422.

Scheme 1. Proposed Oligomerization Mechanisms

Wild Type

$$M + M \longrightarrow M_2 \longrightarrow \text{paranuclei} \longrightarrow \text{protofibrils}$$

Pro^{19} Alloform

$$M + M \longrightarrow M_2 \longrightarrow M_3, M_4 \not\longrightarrow \text{higher-order oligomers}$$

be lost in the dissociation process. The $(H)_2$ peak would be the first member of the protofibril family of structures.[54,55]

These results correlate very well with PICUP cross-linking measurements.[10] In those experiments Pro^{19} alloform was dominated by monomer, dimer, and trimer with a small amount of oligomer in the hexamer range. In contrast, the Aβ42 PICUP results indicate a strong monomer, weak dimer and trimer, strong signals from tetramer through hexamer, and finally significant higher-order oligomer. The agreement between the PICUP experiments and the IMS/MS results supports the conclusion that each method reflects accurately the solution-phase oligomerization states of Aβ.

Of note, when Aβ42 is sprayed without filtering out higher-order aggregates (seeds), the mass spectrum is dominated by monomer (−3 and −4 charge states), and there is no evidence from either ATD or cross section measurements that oligomers are present in our mass range (∼3000 amu). However, under these spray conditions, the nanospray tip rapidly clogs, indicating an active aggregation process is occurring. In contrast, when large assemblies are filtered out, a robust −5/2 charge state signal appears in the mass spectrum (Supporting Information). This peak contains a series of oligomers beginning with the dimer and ending with $(H)_2$. These observations are completely consistent with the model proposed by Bitan, Teplow, and coworkers[10] based on PICUP results that suggest Aβ42 monomers are in steady state with paranuclei (pentamers and hexamers) and perhaps even with protofibrils (long chains of paranuclei). Our results allow a modest refinement of this model for the Aβ42 system considered here (Scheme 1).

The Pro^{19} alloform readily forms dimers, trimers, and tetramers, but further oligomerization is very slow or nonexistent. The solutions spray continuously for long periods of time. In contrast, the Aβ42 species forms dimer; however, once it does, it will rapidly oligomerize to the hexamer (and beyond). Further aggregation to large insoluble oligomers is apparently facilitated by (large) oligomers because filtering them out allows sustained spraying of the solution for Aβ42 and observation of the smaller oligomers.

Qualitatively, the difference in the Aβ42 and [Pro^{19}]Aβ42 systems must be due to the disruption in the central hydrophobic cluster (CHC) caused by the F19P substitution. Naturally occurring substitutions in and near the CHC (A21G, E22Q, E22G, E22K, D23N) of Aβ are known to lead to AD diseases and cerebral amyloid angiopathy (CAA).[15−20] The mechanistic basis for the similarity to AD or CAA of the resulting diseases are not known but could be linked to similarities or differences in aggregation kinetics, aggregate structure, or biological function/behavior. Whereas these various CHC substitutions do not block fibrillization, the F19P substitution inhibits it.[21,22] From our data and the earlier PICUP studies, the fibrillization block for [Pro^{19}]Aβ42 appears to occur early in the oligomerization process. The theoretical modeling we have done on Aβ42 indicates that interaction of the CHC with the hydrophobic tail is conserved in virtually all structures while almost all other structural features vary.[45] The F19P substitution may disrupt this conserved interaction, possibly leading to different structures for the dimer and higher-order oligomers. *In silico* studies now in progress will address these possibilities.

The temperature dependence of the −5/2 charge state ATD of [Pro^{19}]Aβ42 allowed Arrhenius parameters to be extracted for dissociation of both the tetramer and the dimer. The activation energies are similar (18.3 and 20.4 kcal/mol for the tetramer and dimer, respectively). These values are substantial for noncovalent complexes, suggesting that side-chain packing contributes to the activation energy. The very low *A* factors (corresponding to entropies of activation of about −56 cal mol^{-1} K^{-1}) suggests a tight transition state for dissociation for both the dimer and tetramer, consistent with unraveling of the side-chain packing.

Conclusions

1. Both Aβ42 and [Pro^{19}]Aβ42 monomer peptides retain solution-based structures when sprayed and analyzed using IMS/MS.

2. A minor fraction of the monomer refolds during the spray/detection process into a lower-energy solvent-free family of conformers.

3. Abundant dimers, trimers, and tetramers are observed for [Pro^{19}]Aβ42. These species do not oligomerize further under the experimental conditions used here, consistent with the fact that [Pro^{19}]Aβ42 does not form amyloid fibrils.

4. Studies of the temperature dependence of the dissociation of both the tetramer and dimer of the −5/2 charge state of [Pro^{19}]Aβ42 allowed Arrhenius factors to be measured. These factors suggest side-chain packing of the monomers in these oligomers, rather than simple van der Waals interactions.

5. Essentially no dimers or higher-order oligomers were observed for freshly dissolved Aβ42 samples even though significant monomer signals were present. However, these solutions rapidly clogged the nanospray tips, indicating very large oligomers were present. This observation is consistent with mechanisms where monomer is in steady state with larger oligomers but *not* with smaller ones (dimer/tetramer). Tip clogging was not observed for [Pro^{19}]Aβ42 even for extended sampling times (weeks). Thus, higher-order oligomers do not form in [Pro^{19}]Aβ42 under the experimental conditions used here.

6. When Aβ42 peptide was subjected to filtration to remove large assemblies and immediately sprayed, a new peak at −5/2 charge state was observed. This solution could be sprayed for several days, indicating very large oligomers did not form rapidly. These results are consistent with large oligomers facilitating the fibrillization process.

7. The filtered Aβ42 sample contained not only dimers but also abundant tetramers, hexamers, and pairs of hexamers, indicating the first steps toward protofibril formation. This result is consistent with photochemical cross-linking (PICUP) experiments.

8. Molecular modeling indicates that interaction of the hydrophobic cluster (residues 17−21) and hydrophobic tail (residues 29−42) occurs in the −3 monomer.[45] The gas-phase structure is turned "inside out" relative to the solution structure

(54) Walsh, D. M.; Lomakin, A.; Benedek, G. B.; Condron, M. M.; Teplow, D. B. *J. Biol. Chem.* **1997**, *272*, 22364−22372.
(55) Harper, J. D.; Wong, S. S.; Lieber, C. M.; Lansbury, P. T. *Chem. Biol.* **1997**, *4*, 119−125.

and is much more compact. The difference in cross section between the two structures correlates well with the experiment.

Acknowledgment. We thank Megan Grabenauer and Dr. James Pavlovich for assistance with some of the experiments, Margaret M. Condron, Sabrina Vollers, and Sean Spring for peptide synthesis and preparation, and Dr. Catherine Carpenter for help organizing and writing the manuscript. M.T.B. gratefully acknowledges the National Science Foundation and the Air Force Office of Scientific Research for equipment support. D.B.T. acknowledges support from the NIH (NS38328, NS44147, AG18921) and the Foundation for Neurologic Diseases. J.-E. S. thanks the David and Lucile Packard Foundation for support.

Supporting Information Available: Additional mass spectra and arrival time distributions for Aβ42. This material is available free of charge via the Internet at http://pubs.acs.org.

JA044531P